ACS OMEGA

http://pubs.acs.org/journal/acsodf

Article

Tuning the Emission Wavelength of Lead Halide Perovskite NCs via Size and Shape Control

Junfu Leng, Tian Wang, Zhi-Kuang Tan, Ya-Ju Lee, Chun-Chieh Chang, and Kaoru Tamada*

Cite This: *ACS Omega* 2022, 7, 565−577

Read Online

ACCESS | Metrics & More | Article Recommendations | Supporting Information

ABSTRACT: The advent of lead halide perovskite nanocrystals (NCs), which are easily synthesized, ultralow-cost materials and have an impeccable luminous efficiency, has drastically changed the future perspective of semiconductor quantum dot devices. Although the band gap energy of lead perovskite NCs can be tuned by the halide composition, the instability problem prevails for mixed-halide perovskite NCs, caused by phase segregation due to ion migration when an external electric field or light is applied. To avoid this problem and obtain the stable emission of RGB primary colors, in this study, two synthesis pathways of pure-halide perovskite NCs are proposed. One approach is the modified hot injection method with "centrifugation of a frozen eutectic mixture" to separate small NCs efficiently, and the other is the "low-temperature mixing and heat-up method" for target materials including $CsPbI_3$, $CsPbBr_3$, and $CH(NH_2)_2PbBr_3$ ($FAPbBr_3$). The emission wavelength of $FAPbBr_3$ is tuned ion-stoichiometrically, unlike Cs perovskites. These various synthesis pathways of pure-halide perovskite NCs enable the efficient production of high-quality perovskite NCs and allow precise tuning of the emission color to the desired wavelength. Although there are still several "gaps" remaining in the available emission wavelength, the new methodology proposed in this study could potentially be employed for manufacturing more stable perovskite NC-based optoelectronic devices.

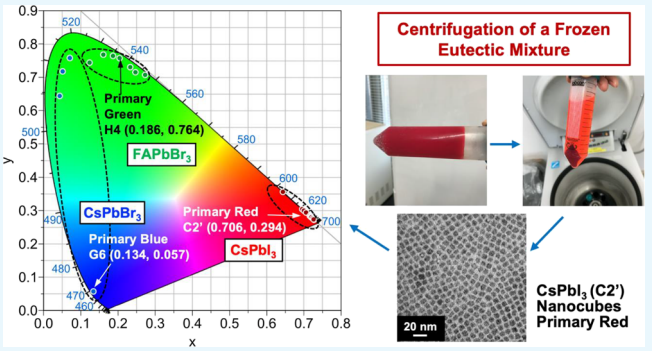

1. INTRODUCTION

Electroluminescent devices and photoelectric conversion devices using solid-state semiconductor materials with a suitable band gap have been developed for light-emitting diode (LED) light sources, displays, solar cells, lasers, etc.[1−4] The physical properties of these semiconductor materials are normally controlled by doping impurities, and the performance of the resulting semiconductor devices is constantly improving with advances in nano-/microfabrication techniques. Apart from solid-state semiconductors, colloidal semiconductor nanocrystals (NCs), also known as colloidal quantum dots (QDs), have also attracted considerable attention in recent years as alternative powerful components for semiconductor devices.[5]

When the size of optical and electronic materials decreases to the range of 1−100 nm, certain materials would exhibit altered properties according to their size and shape, which results in various band gap ranges.[6] By combining the chemical composition and the size/shape of QDs, wide-emission colors covering ultraviolet to near-infrared have been obtained, satisfying various industrial needs.[7−9]

QDs have narrow, wavelength-adjustable emission and excellent luminous efficiency and can provide accurate color performance in high-brightness displays. Compared with organic LED TVs, which are currently high-end products, QD TVs have better color performance, longer service life, and lower production cost.[10,11] The representative colloidal QDs are II-VI semiconductor NCs such as cadmium chalcogenides,[12] and some of others from III-V or I-III-VI_2 semiconductor NCs have been developed.[3,9,13] These traditional QDs present common problems concerning sensitivity to surface defects, and surface passivation by core-shell structures is required to obtain stable emission and improve luminous efficiency.[14−16] Therefore, the synthetic procedure of these QDs is inevitably complicated, especially when trying to achieve a lattice-matched core-shell structure.

In recent years, the advent of lead halide perovskite NCs, which are easily synthesized, ultralow-cost materials and have an impeccable luminous efficiency, has drastically changed the future perspective of QD devices.[17−20] The efficiency of light-emitting devices and solar cells using perovskite NCs has caught up with that of traditional QD devices within a short

Received: September 10, 2021
Accepted: November 23, 2021
Published: December 7, 2021

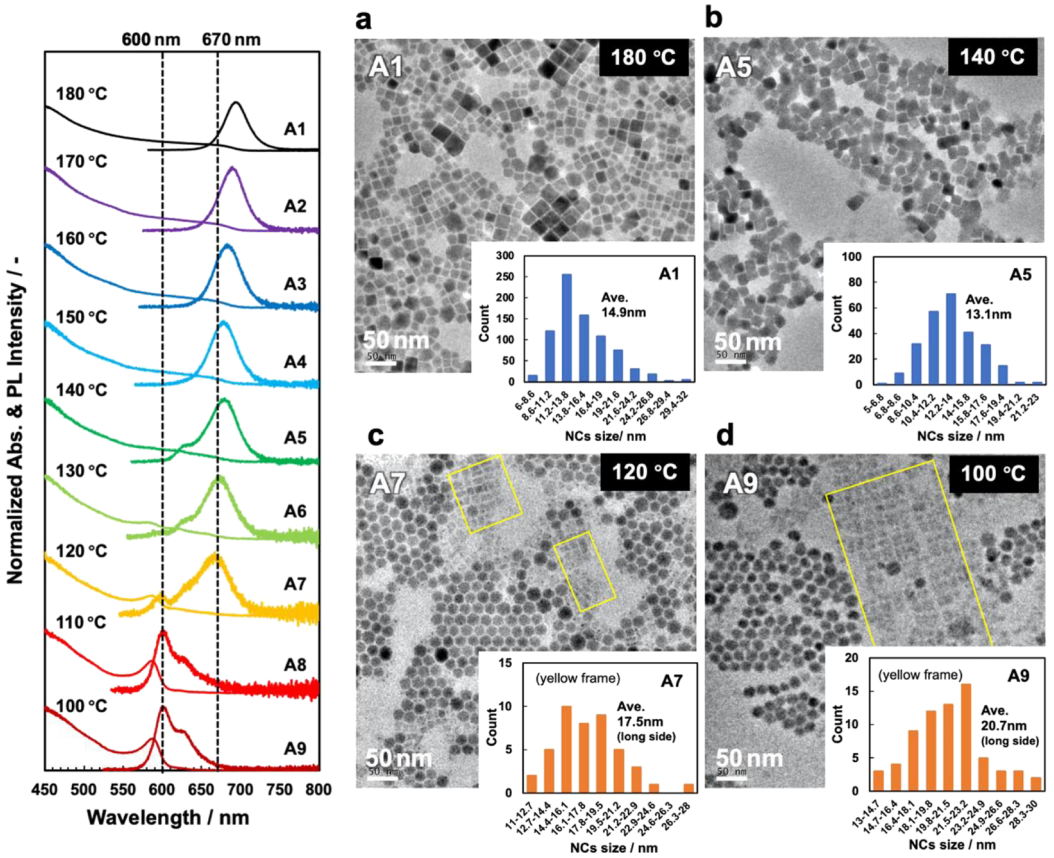

Figure 1. Reaction temperature-dependent PL and absorption spectra (left) and TEM images (right) of $CsPbI_3$ NCs synthesized by the hot injection method (**A1**−**A9**). The shape of NCs at 180 °C (a) and 140 °C (b) is cubic, and those at 120 °C (c) and 100 °C (d) are hexagonal but partly includes square or rectangular nanoplates (in the yellow frames). The insets are the in-plane size distribution of $CsPbI_3$ NCs obtained from the TEM image in the yellow frames. For rectangular nanoplates, the values are obtained from the longer side. The size of hexagonal NCs is not counted.

period.[21,22] All-inorganic lead-halide perovskite $CsPbX_3$ (X = Cl, Br, or I) was synthesized in the early 1950s,[23] but its superior optical properties were not found until 2009. The solar cell with an energy conversion efficiency of up to 3.8% was developed using a metal−organic halide perovskite, methylammonium lead iodide ($MAPbI_3$),[24] and this study has been followed by many other researchers.[17,25] Owing to the success of metal−organic halide NCs, all-inorganic perovskites have received attention again, and $CsPbX_3$ NCs with excellent luminescence properties were reported in 2015.[18] $CsPbX_3$ has a similar structure to $MAPbX_3$ but is more stable and has a higher photoluminescence quantum yield (PLQY) (~90%), a narrow full width at half maximum (FWHM) (12−42 nm), and a wide emission spectrum covering the entire visible wavelength range (400−700 nm).

The band gap energy of these perovskite NCs can be easily tuned by varying the mixing ratio of halogens, which can even be achieved by ion exchange after NC synthesis.[26] However, these mixed-perovskite NCs have low stability under an external electric field or light irradiation,[27,28] where multiple halogen elements inside mixed halide perovskites start showing various reactions and displacements, which leads to phase segregation and decomposition except in some cases.[29] These materials also exhibit an emission spectral shift during photoexcitation or electrical excitation, which impairs the quality of commercial displays that demand stringent reliability standards.[30,31]

To avoid these problems and obtain the stable emission of RGB primary colors that meet the Rec. 2020 standard, in this study, two synthesis pathways of pure-halide perovskite NCs are proposed. One approach is the "modified hot injection method", and the other is the "low-temperature mixing and heat-up method" as our original strategy. These methods are applied for the synthesis of $CsPbI_3$, $CsPbBr_3$, and $CH(NH_2)_2PbBr_3$ ($FAPbBr_3$).

In the hot injection method, the size of the QDs and emission wavelength are generally determined by (i) the preparation conditions for precursors, (ii) the reaction temperature when the precursors are mixed, and (iii) the reaction time after mixing. However, perovskite compounds are highly reactive and nucleation and growth proceed within seconds after mixing,[18] so (iii) controlling the reaction time is practically impossible. Therefore, in this study, we tried to optimize the preparation conditions of the PbX_2 precursor by using ligand molecules. In practice, we lowered the reaction temperature and shortened the reaction time by optimizing the amount of ligand molecules, leading to success in synthesizing small, high-quality NCs even if the mixing temperature of the precursors was as high as that in a standard hot injection method, which was 150 to 170 °C ("modified hot injection method"). In addition, we developed a purification method named "centrifugation of a frozen eutectic mixture" to separate small homogeneous NCs from the reaction mixture, which was used in combination with the modified hot injection method.

https://doi.org/10.1021/acsomega.1c05001
ACS Omega 2022, 7, 565−577

These synthetic methodologies were applied for the synthesis of $CsPbI_3$ (**C1**−**C3**) and $CsPbBr_3$ (**F1**).

The "low-temperature mixing and heat-up method" is developed to separate nucleation and growth processes by lowering the temperature (<40 °C) when precursors are mixed. After mixing, the reaction solution was heated to a certain temperature. In this synthetic method, perovskite NCs grow from one dimension to two dimensions depending on the reaction temperature via a thermodynamically controlled reaction.[32] The emission wavelength of the two-dimensional NCs synthesized by this low-temperature mixing method appeared at a shorter wavelength than that of the three-dimensional NCs synthesized by the hot injection method. These synthetic methodologies were applied for the synthesis of $CsPbI_3$ (**D1**−**D2**) and $CsPbBr_3$ (**G1**−**G6**).

For the case of FA perovskite NCs, the emission wavelength is controlled by the amount of the cation precursor (FA-oleate), where large NCs could be synthesized without raising the temperature. This method solved the problem of instability for FA perovskites in high-temperature reactions (the reaction temperature was 160 °C, so we categorized this method as a "modified hot injection method"). These synthetic methodologies were applied for the synthesis of $FAPbBr_3$ (**H1**−**H8**).

In this study, $CsPbI_3$ (**A1**−**A9** and **B1**−**B9**) and $CsPbBr_3$ (**E1**−**E4**) were synthesized by conventional methods (hot injection method + centrifugation or antisolvent-assisted precipitation method). We found a couple of interesting phenomena through the experiments by evaluating a wide range of reaction conditions, which led to the idea of the original "low-temperature mixing and heat-up method" mentioned above. A series of lead−halide perovskite NCs synthesized in this study is summarized in the Supporting Information.

2. RESULTS AND DISCUSSION

2.1. Synthesis of $CsPbI_3$ by the Hot Injection Method: Effect of Reaction Temperature and Reaction Time (Samples A1−A9). The synthesis of $CsPbI_3$ NCs was conducted by the conventional hot injection method. Figure 1 shows the reaction temperature-dependent PL and absorption spectra of $CsPbI_3$ NCs. The reaction time was 5 s for all experiments. The PL wavelength of the 180 °C sample was 699 nm, which is close to the bulk crystal PL wavelength of 717 nm (1.73 eV). The PL and absorption wavelengths exhibited a blueshift as the reaction temperature decreased, i.e., as the NC size decreased. However, the low-temperature reaction below 150 °C was not homogeneous as observed by the broadened PL spectra. When the reaction temperature was 110 °C or below, the PL peak position changed to 600 nm. Interestingly, a large gap in the PL wavelength between 600 and 670 nm appeared for such a small temperature change.

Figure 1a−d shows Transmission electron microscopy (TEM) images of $CsPbI_3$ NCs synthesized at various temperatures. The NCs synthesized at 180 °C (Figure 1a) and 140 °C (Figure 1b) exhibited a square (cubic) structure as a main component. Upon careful examination, the products at 180 °C exhibited a clear boundary between the NCs, while those at 140 °C appeared to be partly fused. This observation implies that 140 °C is the critical temperature for the stable formation of cubic $CsPbI_3$ NCs. Although a small shoulder peak appeared at 140 °C, small NCs were not confirmed in the TEM images. At 120 °C (Figure 1c) and 100 °C (Figure 1d), the main crystalline structure changed from cubic to hexagonal. Figure 1c,d includes square- or rectangular-shaped nanoplates with thicknesses of a few nanometers (observed as a low-contrast image) in the yellow-marked frames. These hexagonal NCs are known as a typical perovskite derivative with a wide band gap, Cs_4PbI_6, generally formed by synthesis with an excessive amount of Cs-oleate precursor (see Figure 2c).[33]

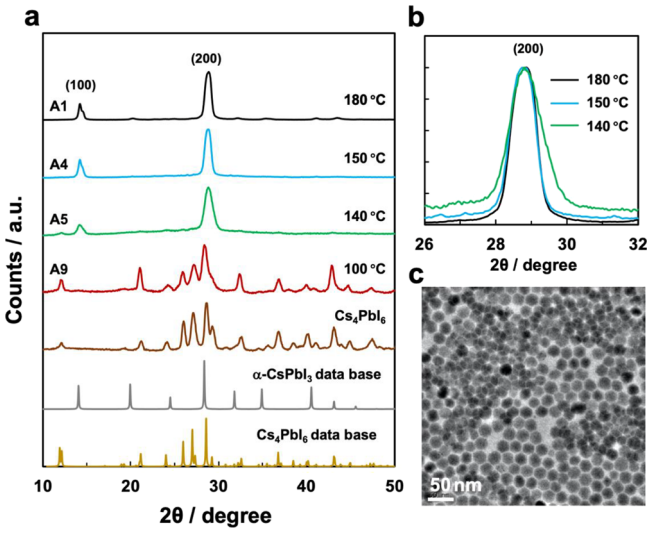

Figure 2. (a) XRD data of $CsPbI_3$ NCs synthesized by the hot-injection method (drop-cast film) at 100−180 °C (**A1**, **A4**, **A5**, and **A9**). For comparison, the Cs_4PbI_6 NCs synthesized by using excess Cs-oleate precursor (five times the amount) and the databases of the bulk perovskites (α-$CsPbI_3$ and Cs_4PbI_6) are shown together. (b) Magnified (200) facet signals. (c) TEM image of Cs_4PbI_6 NCs synthesized by using excess Cs-oleate precursor.

Although this is an undesired material with no emission of visible light, the production of Cs_4PbI_6 NCs via low-temperature synthesis is a newly found phenomenon. The short-wavelength PL of the low-temperature NCs (**A7**−**A9**) likely originates from the nanoplates in the yellow-marked frames in Figure 1c,d. These nanoplates were thin, but the in-plane size was larger than the cubic $CsPbI_3$ NCs.

Figure 2a presents the result of X-ray diffraction (XRD) analysis of sample A (**A1**, **A4**, **A5**, and **A9**) in comparison with Cs_4PbI_6 NCs synthesized by using excess Cs-oleate precursor (five times the amount) and the databases of bulk perovskites (α-$CsPbI_3$ and Cs_4PbI_6). The data clearly confirmed that the 180 °C (**A1**), 150 °C (**A4**), and 140 °C (**A5**) products are cubic. Unlike in the bulk crystals, here, only the signals on the (100) and (200) facets were detected, which was slightly shifted to the larger angles compared with the α-$CsPbI_3$ data base, suggesting a small lattice constant compared with the bulk materials. On the other hand, the XRD result of the 100 °C product (**A9**) perfectly agreed with those of Cs_4PbI_6 NCs and bulk Cs_4PbI_6, which supports our assumption that the hexagonal NCs formed at low temperatures are Cs_4PbI_6. Since the Cs_4PbI_6 NCs are rigid and stable, the XRD peak positions well agreed with that of bulk data. The amount of α-$CsPbI_3$ was very little compared to Cs_4PbI_6 as shown in the TEM image (Figure 1d); the XRD spectra of A9 appeared about identical to that of Cs_4PbI_6 NCs (main component).

Figure 2b shows the magnified (200) facet signals of 180, 150, and 140 °C products. As the reaction temperature decreased, the peak FWHM broadened, i.e., the size of the

https://doi.org/10.1021/acsomega.1c05001
ACS Omega 2022, 7, 565−577

NCs must decrease as the reaction temperature decreases according to the following Scherrer equation

$$\tau = \frac{K\lambda}{\beta \cos\theta} \quad (1)$$

Here, τ is the mean size of the crystalline material, K is the shape factor, λ is the X-ray wavelength, β is the peak FWHM, and θ is the Bragg angle. This result is consistent with the blueshifted PL spectra and the TEM images shown in Figure 1.

Figure 3 shows the influence of reaction time (the time after cationic precursor injection and before quenching). When

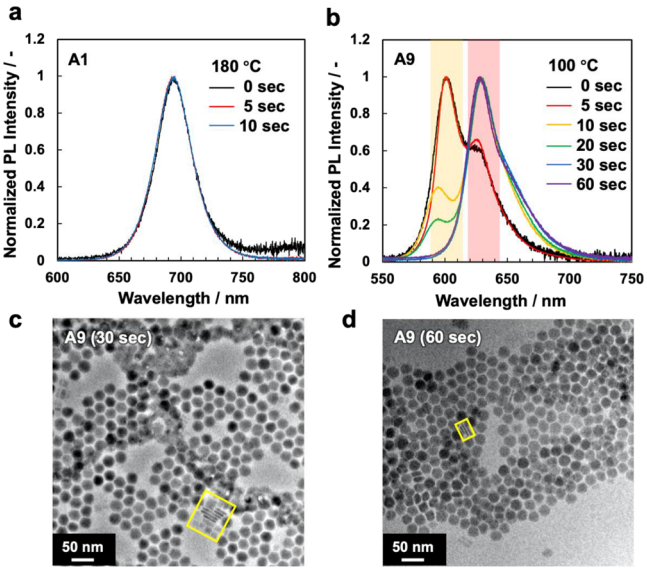

Figure 3. Reaction time-dependent PL spectra of sample **A** synthesized at (a) 180 °C (**A1**) and at (b) 100 °C (**A9**). TEM images of the NCs synthesized at 100 °C for (c) 30 s and (d) 60 s. The main product was hexagonal Cs_4PbI_6 NCs, but $CsPbI_3$ nanoplates were also found in the yellow frames (thickness was determined to be 4.5−5 nm).

$CsPbI_3$ NCs were synthesized at a high temperature (180 °C), the emission spectra of the products synthesized with different reaction times overlapped as shown in Figure 3a. The large noise in the spectra of the 0 s product suggests a lower PLQY (Here, the reaction time "0 s" means that the flask was placed in ice water immediately after injection of the Cs-oleate precursor). This means that the reaction time in the range of a few seconds has little influence on the product.

The data show that the influence of reaction time increases for the synthesis at low temperatures. The PL spectra shown in Figure 3b exhibited two peaks at 600 and 630 nm, marked by orange and red bands. As the reaction time increased from 0 to 30 s, the PL intensity at 600 nm gradually decreased while the PL intensity at 630 nm increased. The data at 0 and 5 s did not show a significant difference, which may be due to the experimental error given such a short reaction time. The data at 30 and 60 s appeared the same, both of which had an emission peak only at 630 nm. The TEM images in Figure 3c (30 s) and Figure 3d (60 s) were also identical. This result suggests that the reaction was completed at 30 s and the main product of the low-temperature reaction was hexagonal Cs_4PbI_6 NCs regardless of whether the reaction time was long or short. As mentioned earlier, hexagonal Cs_4PbI_6 NCs are a material with no visible emission, and the emission found in the PL spectra likely originates from the nanoplates marked by yellow frames in the same way, as shown in Figure 1c,d. As presented in Figure 1, the PL wavelength of low-temperature and short-reaction time products (100−120 °C; reaction time, 5 s) appeared at 600 nm for nanoplates in the "face-up" arrangement. On the other hand, as shown in Figure 3, the PL wavelength of low-temperature and long-reaction time products (100 °C; reaction time, 30−60 s) appeared at 630 nm for nanoplates in a stacked and vertically aligned structure. The thickness of the nanoplates was estimated to be 4.5−5 nm, corresponding to a seven- or eight-layer thickness of $CsPbI_3$ unit cells.

By a series of experiments, we confirmed that the PL peak position could be tuned by the reaction time and temperature even by the hot injection method. However, a PL wavelength gap between 630 and 670 nm remains. This means that the ideal primary color of red at approximately 650 nm as our target could not be achieved by this conventional hot injection method. This problem could be solved as described in the following section.

2.2. Purification of $CsPbI_3$ by the Antisolvent-Assisted Precipitation Method (Samples B1−B9). As the reaction temperature decreased, the amount of products isolated by centrifugation decreased, and the color of the supernatant intensified (Figure S1 in the Supporting Information). This result indicates that a large amount of product remained in the reaction mixture solution, which should be smaller NCs. On the other hand, when NCs were synthesized at 110 °C or below, a large amount of NCs precipitated and the supernatant was less colored. The reason is likely that the products changed from $CsPbI_3$ to Cs_4PbI_6 at this temperature as suggested by the TEM and XRD data.

The technique of adding an antisolvent (usually polar solvents such as acetonitrile, acetone, butanol, methyl acetate (MA), or ethyl acetate (EA)) to the reaction solvent of 1-octadecene (ODE) to accelerate the precipitation of products has been reported.[18,34−36] However, polar solvents are usually destructive to perovskite NCs. Therefore, this is a risky approach and requires careful selection of the appropriate solvent and dosage. We found that a small amount of acetone or butanol caused the decomposition of $CsPbI_3$ NCs. On the other hand, an appropriate amount of MA and EA promoted the precipitation of small NCs.

Absorption and PL spectra of the $CsPbI_3$ NCs (sample **A**) purified with EA-assisted precipitation are shown in Figure 4a (sample **B**). The shape of the PL spectra became smooth and symmetric by EA-assisted precipitation. The PL wavelength of the product synthesized at 120−100 °C changed continuously between 650 and 690 nm, unlike sample **A** in Figure 1. The PL wavelength could also be adjusted by the dosing amount of EA. Figure 4b shows the spectrum change of the product synthesized at 100 °C with different amounts of EA. Here, 1−5× indicates the volume ratio of EA relative to that of the reaction solvent ODE; 1× corresponds to the addition of 5 mL of EA. As the amount of EA increased, the peak at 600 nm first shifted to 630 nm for 1× and then eventually to 650 nm for 5×. Thus, by adding an appropriate amount of EA (5× for the **B9** sample), the subpeak materials could be removed. Furthermore, the 650 nm emission corresponding to the ideal primary color of red is successfully demonstrated, which could not be obtained in the series of sample **A**.

This phenomenon can be interpreted as follows. By the addition of EA, $CsPbI_3$ nanoplates with a larger surface area

https://doi.org/10.1021/acsomega.1c05001
ACS Omega 2022, 7, 565−577

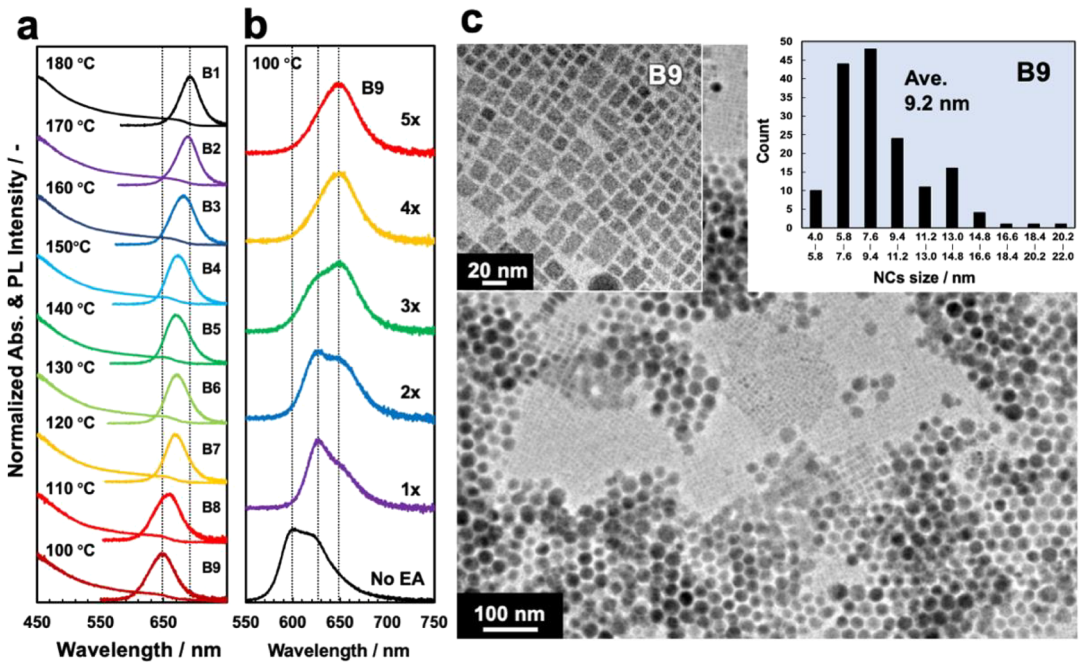

Figure 4. The effect of EA on isolation of the products. (a) PL and absorption spectra of products isolated by using 5× EA (**B1**−**B9**). (b) The influence of the dosing amount of EA on the spectrum of the reaction mixture obtained at 100 °C. Here 1−5× means the volume ratio of EA against the reaction solvent ODE; 1× corresponds to the addition of 5 mL of EA. (c) TEM images of the product synthesized at 100 °C and isolated by using 5× EA. The image confirmed that the hexagonal Cs_4PbI_6 NCs (no luminescent material) still remained. The magnified image of cubic $CsPbI_3$ NCs (left) and the NC size distribution (right) are shown as insets.

become unstable in ODE and transform into nanocubes to reduce their surface energy. In fact, after adding an extra amount of EA, the nanoplates with short emission wavelengths were selectively destructed and only nanocubes with a longer emission wavelength remained in the TEM image (see the left inset in Figure 4c) together with the hexagonal Cs_4PbI_6 NCs. It is also noted that the size distribution of nanocubes increased by this synthesis method (see the right inset in Figure 4c), which is in good agreement with the broad PL spectrum of **B9** (Figure 4b); thus, further improvement in the synthesis methodology is certainly required.

2.3. Synthesis of $CsPbI_3$ by the Modified Hot Injection Method and Centrifugation of a Frozen Eutectic Mixture (Samples C1−C3 and C1′−C3′). As a summary of the previous experiments, we encountered difficulty in isolating NCs with 630−670 nm emissions by controlling the reaction temperature or time. When the reaction temperature was lower than 140 °C, byproducts were formed and the PL spectra exhibited irregular shapes. When the reaction temperature was further lowered to 120 °C or below, hexagonal, nonfluorescent Cs_4PbI_6 NCs (unfavorable) were formed, and they were difficult to remove. Therefore, the feasible reaction temperature should be above 150 °C. However, as shown in Figure S1 in the Supporting Information, small NCs were difficult to isolate by regular centrifugation and remained in the supernatant. To solve this problem, we have developed a new purification methodology named "centrifugation of a frozen eutectic mixture" to isolate small homogeneous NCs.

There have been a couple of related reports using toluene and low temperature to induce the precipitation of NCs.[35,36] Toluene was added to the crude solution after synthesis and kept at low temperature, and impurities were removed by solidification from the pure product. This method was developed to prevent chemical damage to the NC product caused by the addition of polar antisolvents. We tried to use this method to precipitate small NCs from the crude solution. Toluene is a good solvent for NC products encapsulated by nonpolar ligands. However, toluene and the reaction solvent ODE were not perfectly miscible, and they tended to become separated into two phases during the cooling process to −14 °C. The melting point of ODE is 14 °C, so when the solution was chilled, phase-separated ODE was solidified and settled at the bottom of the centrifuge tube. This problem was solved by using hexane instead of toluene. Hexane is also a good solvent for NCs, and its melting point is the same as that of toluene. However, the miscibility of hexane with ODE is higher than that of toluene, so we could obtain a totally solidified mixed solution (frozen eutectic mixture) at −14 °C. By centrifugation of the frozen eutectic mixture, we could isolate small NCs with a high yield. The whole procedure (**a**−**d**) and the obtained PL spectra (**e**) are shown in Figure 5.

The mechanism to isolate small NCs is as follows; during "centrifugation of a frozen eutectic mixture," the hexane or hexane-rich solution with lower freezing point melts before the ODE or ODE-rich solution melts, and the NCs dispersed in this low-viscosity solution precipitates at the early stage of centrifugation. However, when centrifugation is continued, melted viscous solvent and ligands (ODE, oleic acid (OA), and oleylamine (OLA) coprecipitate on top. These extra materials are removed by further centrifugation in hexane without using the freezing method. As summarized in Figure 5f, the repeated purification improved the quality of the NCs. In general, chemical purifications have adverse effects on the stability of perovskite NCs, and the number of purifications should be limited.[18,34,35,37] We found that our method did not damage the NCs and could be performed repeatedly.

Figure 6 shows the morphology and size distribution of the 3× purified small $CsPbI_3$ NCs synthesized at 160 °C. After

https://doi.org/10.1021/acsomega.1c05001
ACS Omega 2022, 7, 565−577

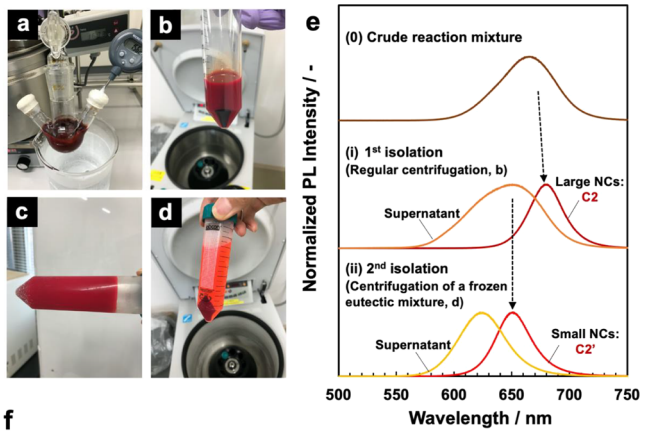

f

(i) 1st isolation: large NCs

Number of Purifications	Emission wavelength (nm)	FWHM (nm)	PLQY (%)
0	683	37	53.3
1	678	36	79.9
2	676	36	97.3
3	675 (C2)	34	97.3

(ii) 2nd isolation: small NCs

Number of Purifications	Emission wavelength (nm)	FWHM (nm)	PLQY (%)
0	662	42	93.1
1	655	39	98.6
2	653	38	97.3
3	652 (C2')	36	97.2

Figure 5. Purification methodology by "centrifugation of a frozen eutectic mixture" for $CsPbI_3$ products (synthesized at 160 °C). (a) The crude reaction mixture solidified by cooling in an ice water bath. The main components are ODE, OA, and OLA. (b) The sample after the first isolation (without freezing). The deep red precipitates are the large $CsPbI_3$ NCs. (c) The solidified supernatant with three volumes of hexane in a −14 °C freezer for 1 h. (d) The sample after the second isolation at −5 °C. A large amount of small NCs are precipitated. (e) The PL spectra of the samples at each isolation process. (f) Emission wavelength, FWHM, and PLQY with the number of purifications for (i) large NCs (**C2**) and (ii) small NCs (**C2′**, primary red).

sufficient purification, the NCs showed good dispersibility and a small size distribution. A single-NC high-resolution (HR)-TEM image revealed that the interplanar spacing was 0.62 nm, which corresponds to the (100) facet of cubic phase $CsPbI_3$ consistently with other reports.[35,38] The value of 0.62 nm is slightly smaller than the lattice constant of bulk $CsPbI_3$ (0.64 nm), reflecting nanocrystalline characteristics, which is consistent with the XRD data in Figure 2a.

For the synthesis of small $CsPbI_3$ NCs, we modified the hot injection method to improve the yield. As mentioned above, we found that the preparation condition of the lead iodide precursor significantly influences the product, especially for the case of reaction temperatures below 170 °C. The color of the precursor solution gradually deepened from nearly colorless light yellow to dark yellow during heating to 120 °C. Upon further heating to 150 °C, the solid lead iodide salt tended to be reprecipitated. This result indicates that the monomer concentration reached critical solubility at high temperatures. We also found that a high-concentration precursor solution tends to form large particles with a relatively uniform size, which is suitable for the synthesis of NCs with PL wavelengths above 680 nm but not suitable for the synthesis of small NCs. Based on this knowledge, we shortened the heating time of the lead iodide precursor and simultaneously optimized the amount of ligands (OA and OLA) to maintain a proper concentration of the precursor at high temperatures. As ligands, OA accelerates the formation of precursors and OLA increases monomer solubility. A detailed discussion of the role of solvent and ligands is available in Figure S2 in the Supporting Information. This modification of the synthesis conditions led to a slight blueshift of the PL wavelength of the first isolated NCs and a reduced yield, while the yield of the small, second isolated NCs was increased. By combining this modified hot injection method and the purification by "centrifugation of a frozen eutectic mixture", we obtained $CsPbI_3$ NCs with 643−680 nm emission wavelengths at reaction temperatures of 150−170 °C, as shown in Figure 7a (samples **C1**−**C3** and **C1′**−**C3′**).

2.4. Synthesis of $CsPbI_3$ by the Low-Temperature Mixing and Heat-Up Method (Samples D1 and D2). We found that the reaction solution did not change color instantly after mixing when the Cs-oleate precursor was injected at a lower temperature such as 60 °C. However, if the reaction mixture solution was heated for a period of time (more than 1 min), the solution started to color gradually. After 3 min of

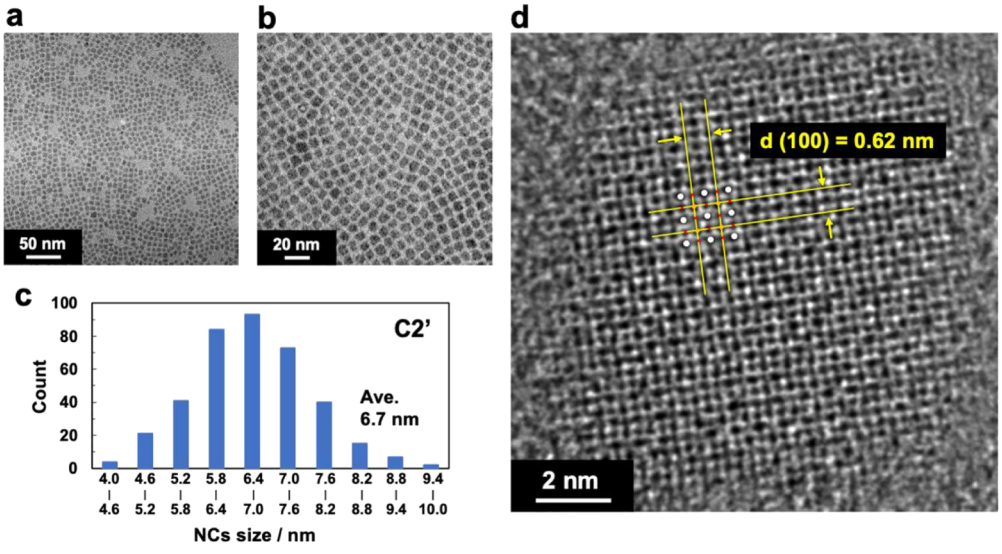

Figure 6. (a) TEM image of 3× purified $CsPbI_3$ NCs synthesized at 160 °C and (b) the magnified image. (c) The size distribution obtained from the TEM image of (b). (d) HR-TEM image of a $CsPbI_3$ single crystal. The interplanar spacing of 0.62 nm corresponds to the (100) facet. The possible atomic (column) arrangement is marked by three colors: white, Cs; blue, Pb; red, I.

https://doi.org/10.1021/acsomega.1c05001
ACS Omega 2022, 7, 565−577

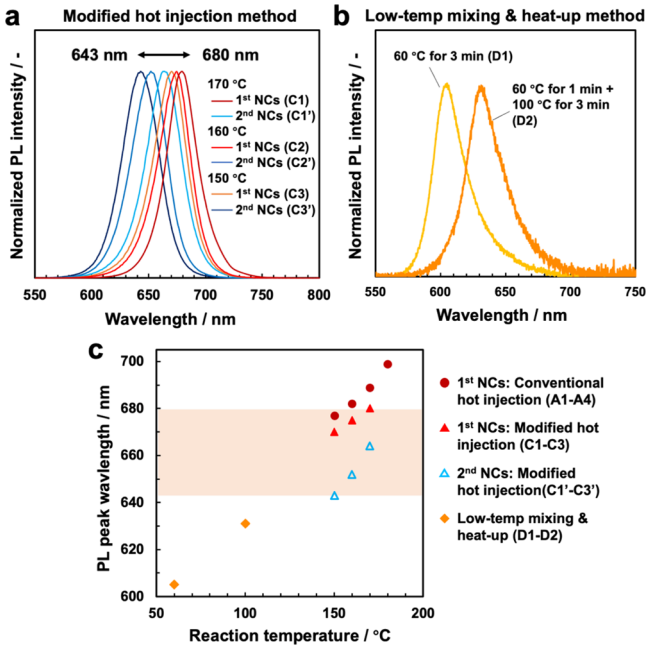

Figure 7. (a) PL spectra of $CsPbI_3$ NCs synthesized at 150−170 °C by the modified hot injection method (**C1**−**C3** and **C1′**−**C3′**). (b) PL spectrum of $CsPbI_3$ NCs synthesized by low-temperature and heat-up methods by injecting the Cs-oleate precursor solution at 60 °C (**D1**−**D2**). (c) Summary of the emission wavelength of $CsPbI_3$ NCs. The spherical red marks are the NCs synthesized by the original hot injection method (**A1**−**A4**). Products synthesized below 150 °C by the hot injection method are omitted from the plots because of unstable, multiple emissions.

reaction, the color change was almost saturated as detected by the naked eye (Figure 7b, yellow line). When the reaction proceeded at 100 °C for 3 min after injecting the Cs-oleate precursor at 60 °C for 1 min, we obtained a product with a slightly longer wavelength (Figure 7b, orange line). The PL wavelengths of these two products (**D1** and **D2**) are 605 and 631 nm, respectively, which are approximately the same as those of $CsPbI_3$ nanoplates obtained by the hot injection method at 100 °C (Figure 3b, **A9**). The difference is that the conventional hot injection method at 100 °C produced a mixed product with multiple emission wavelengths even at 0 min reaction time, while the products here at 60 °C showed a single peak suggesting uniformly sized 2D nanoplates, and the wavelength could be tuned by heating at 100 °C via a controlled slow reaction process. For the conventional hot injection method at high temperature, nucleation is completed in an extremely short time, and then, 3D crystal growth continues spontaneously (in seconds). This process brings difficulty in controlling crystal grain size and uniformity. In contrast, the low-temperature mixing method provides a breakthrough for size and shape control of the $CsPbI_3$ NCs, although the obtained PL wavelength was too short against the target primary red (wavelength 650 nm). This low-temperature mixing and heat-up method was suitable to obtain the primary blue color (460 nm) for $CsPbBr_3$ as reported in our previous paper.[32] The mechanism of color control by this low-temperature crystal growth is explained in a later section for $CsPbBr_3$.

2.5. Synthesis of $CsPbBr_3$ by the Hot Injection Method (Samples E1−E4). $CsPbBr_3$ is the most widely studied material among inorganic pure-halide perovskite NCs. The typical PL wavelength of $CsPbBr_3$ NCs is ∼510 nm, and they are used as green luminescent materials in most studies and commercial materials. However, $CsPbBr_3$ could not provide luminescence wavelengths greater than 520 nm even with size control, although the wavelength of primary green light was approximately 530 nm.[34] Therefore, this study aimed to obtain the blue primary color emission from $CsPbBr_3$ NCs by reducing the size of the NCs.

Similar to $CsPbI_3$ NC synthesis, we used a hot injection method at a lower temperature. Figure 8 shows the reaction

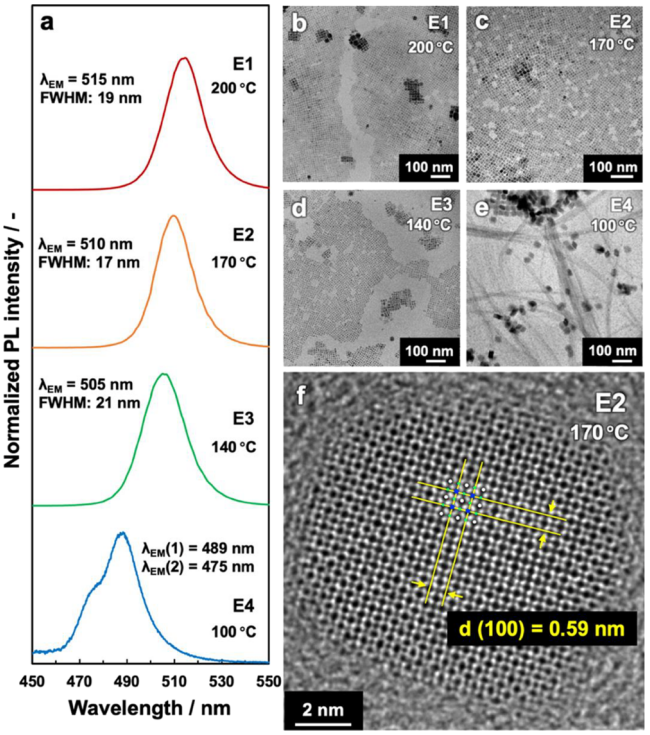

Figure 8. (a) Reaction temperature-dependent PL spectra. TEM images of $CsPbBr_3$ NCs synthesized at (b) 200 °C, (c) 170 °C, (d) 140 °C, and (e) 100 °C (samples **E1**−**E4**). (f) HR-TEM image of a $CsPbBr_3$ single NC synthesized at 170 °C. The interplanar spacing of 0.59 nm indicates the (100) facet. The possible atomic (column) arrangement is marked by three colors: white, Cs; blue, Pb; green, Br. Absorption spectra of **E1** and **E2** are available in Figure S3 in the Supporting Information.

temperature-dependent PL spectra and morphologies of the obtained $CsPbBr_3$ NCs. The PL wavelengths of the $CsPbBr_3$ NCs were blueshifted as the reaction temperature decreased to 200, 170, and 140 °C (Figure 8a). The TEM image in Figure 8b−d reveals that all reactions formed nanocubes. Although the centrifugation conditions were the same for all reaction crude solutions, the product synthesized at 200 °C included large, thick NCs (dark domains), as shown in Figure 8b, which suggests the difficulty of controlling the nucleation and growth processes at high temperatures. In fact, this is the maximum size that can be obtained as a colloidal dispersion. For such large NCs, the PLQY was reduced due to the weakening of the quantum confinement effect and exciton binding energy; hence, these are not desired luminescence materials.

The NCs synthesized at 170 °C exhibited the narrowest FWHM, corresponding to the smallest size distribution, as shown in Figure 8c. The PL wavelength was 510 nm, which is a typical value for $CsPbBr_3$ NCs reported in most studies. For

https://doi.org/10.1021/acsomega.1c05001
ACS Omega 2022, 7, 565−577

the NCs synthesized at 140 °C, the morphology again became nonuniform (Figure 8d), where the length and width of some NCs were different from those of the original cubes. The NCs synthesized at 100 °C were completely different from the other NCs and included two large-grained polygons with different shapes and nanowires (Figure 8e). NCs with a square shape are likely orthorhombic-phase $CsPbBr_3$ (direct-band gap semiconductor), while those with a rhombus shape are likely Cs_4PbBr_6 (wide-band gap insulator).[33] These are the products that typically appear at low temperatures.[39] Thus, the largely blueshifted multiple PL spectrum for 100 °C NCs likely originates from other small structures that were not visible in the TEM images. It should be noted that even if the reaction temperature decreased from 200 to 100 °C, the PL peak position did not reach the ideal blue color (~460 nm) by the conventional hot injection method. The lattice constant of orthorhombic-phase NCs is well agreed with the bulk value (Figure 8f).

2.6. Synthesis of $CsPbBr_3$ by the Modified Hot Injection Method and Centrifugation of a Frozen Eutectic Mixture (Samples F1 and F1′). We have tried the "modified hot injection method" and "centrifugation of a frozen eutectic mixture" in the same way as for samples **C1**−**C3** and **C1′**−**C3′**. Here, the preparation time of the lead bromide precursor was shortened to 30 min (half the original reaction time). We used a reaction temperature of 170 °C, which was the temperature that produced the most homogeneous NCs in the conventional hot injection method (Figure 8c). Because the dissolution rate of lead bromide below 100 °C is significantly slower than that of lead iodide, we could not use stepwise heating starting from 60 °C in the case of $CsPbBr_3$ NCs. Instead, here we employed continuous heating (lead bromide was dissolved in the middle of heating before reaching 100 °C). The reaction time at 100 °C was 3 min. The PL spectral data of $CsPbBr_3$ NCs obtained by this modified synthetic method are shown in Figure 9 (samples **F1** and **F1′**).

The synthetic result of $CsPbBr_3$ NCs basically reproduced that of $CsPbI_3$ NCs. By reducing the heating time of the lead bromide precursor solution, the PL wavelength of the product was slightly blueshifted and the FWHM increased. However, the amount of small $CsPbBr_3$ NCs obtained by the second precipitation was much less than that of $CsPbI_3$ NCs, and the PL wavelength of the second isolated NCs was 480 nm (sky blue), which is the wavelength not attainable by the conventional hot injection method, albeit still longer than the target wavelength of 460 nm (right blue). The PLQY of these blue-emitting $CsPbBr_3$ NCs was 41.8%.

2.7. Synthesis of $CsPbBr_3$ by the Low-Temperature Mixing and Heat-Up Method (Samples G1−G6). The result of the synthesis of $CsPbBr_3$ by the low-temperature mixing and heat-up method has already been published in our previous paper,[32] so here, we mainly explain our concept instead of the experimental details: how to control the nucleation and growth process of NCs and obtain monodispersed small NCs by this method.

As described above, the speed of the nucleation and growth of perovskite NCs is quite fast, and it is difficult to control the reaction over time for the conventional hot injection method.[40] We found that the low-temperature reaction of $CsPbI_3$ NCs was sufficiently slow (e.g., 3 min); however, the PL property did not depend on the reaction time but rather on the reaction temperature. It seems that the reaction was no longer

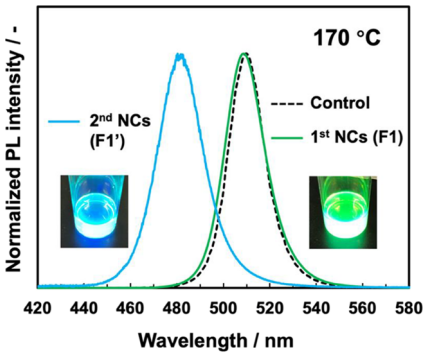

	λ_{EM} (nm)	FWHM (nm)
Control	510	17
1st isolated NCs (F1)	508	20
2nd isolated NCs (F1')	480	23

Figure 9. PL spectra of $CsPbBr_3$ NCs synthesized by the modified hot injection method at 170 °C. The black dotted line represents the product synthesized by the conventional hot injection method as a control experiment. The green line represents the first isolated NC, and the sky blue line represents the second isolated NC from the supernatant. The inset images show the fluorescence color of NC dispersions under UV light. The bottom panel shows a summary of the PL peak position and FWHM of the $CsPbBr_3$ NCs (samples **F1** and **F1′**).

kinetically controlled but thermodynamically controlled in chemical equilibrium. The PL wavelength of $CsPbBr_3$ NCs synthesized by this method showed a large blueshift compared with that of the NCs synthesized by the hot injection method. The blueshift was too large for $CsPbI_3$ to obtain the target primary red color, but it was just the desired level for $CsPbBr_3$ to obtain the target primary blue color. As shown in Figure 10a, a blue emission color of 462 nm was successfully obtained by optimizing the reaction temperature to 140 °C. We also found that the yield could be improved by using the OA and OLA ligands as the reaction solvent instead of ODE (improved five times).

Figure 10b shows the PL spectrum change and scanning transmission electron microscopy (STEM) images during the reaction under heating from 55 to 140 °C. When the reaction started, the PL wavelength was 445 nm, which gradually redshifted to 462 nm by 3 min of reaction (final product: **G6**). The morphology of NCs was also changed from small dot-like NCs to nanorods (3.9 nm wide and 20 nm long; TEM image at 100 °C in Figure 10b) and then stacked "nanostrips" (quasi-2D NCs with 12 nm width and 3 nm thickness, TEM images at 140 °C in Figure 10b,c) by growth. Density functional theory (DFT) calculations in our previous study reasonably interpreted the optical characteristics of the nanorods and nanostrips in consideration of 1D (nanorods) and 2D (nanostrips) confinement effects on the electronic band gap of $CsPbBr_3$.[32] For example, the asymmetric feature of the PL spectrum with a wide "hem" at longer wavelengths is due to asymmetric quantum confinement caused by different electric transitions perpendicular or parallel to the line or plane of low-dimensional materials. The PL spectrum data of samples **G1**−**G5** were obtained by a 3 min reaction at each temperature (the spectrum values were not identical to the data in Figure 10b).

The HR-TEM image in Figure 10c (left) shows the stacked structure of nanostrips with a 5 nm pitch with ligands. Figure 10c (right) shows the lattice spacing of 0.58 nm, which corresponds to the lattice constant of cubic $CsPbBr_3$ in (100)

https://doi.org/10.1021/acsomega.1c05001
ACS Omega 2022, 7, 565−577

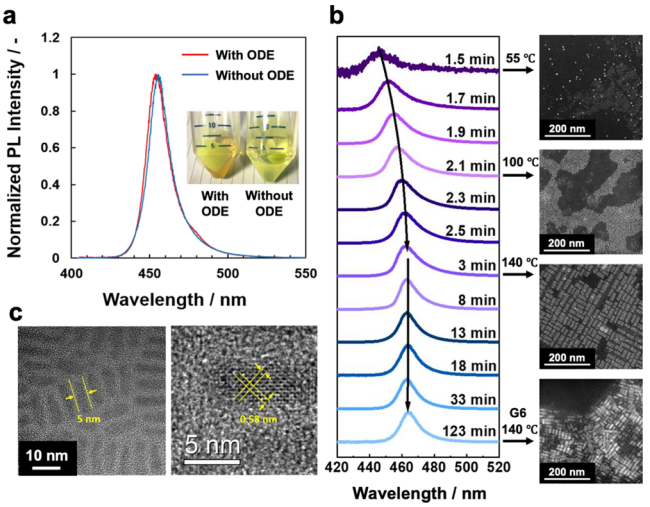

Figure 10. (a) PL spectra of $CsPbBr_3$ NCs synthesized by low-temperature mixing (start temperature: 40 °C) and the heat-up method (final temperature: 140 °C) with/without ODE solvent. The inset image shows the $CsPbBr_3$ NC products obtained by centrifugation (the yield is ca. five times improved with ODE). Left, high yield of NCs synthesized without ODE solvent (only OA and OLA); right, low yield of NCs synthesized with 5 mL of ODE solvent. (b) PL spectrum change and STEM images during the heating process from 55 to 140 °C. (c) HR-TEM images of $CsPbBr_3$ nanostrips stacked by self-assembly. The width and thickness of nanostrips obtained from the image are 12 and 3 nm, the stacked distance with ligands was 5 nm (left), and the lattice spacing was 0.58 nm (right) (**G6**, primary blue).

in good agreement with the XRD data.[32] The lattice constant of the nanostrips was slightly smaller than that of the nanocubes (0.59 nm, Figure 8).

As important information, even if the reaction time was extended for another 2 h, no further spectrum change appeared. This is because the growth of NCs was controlled thermodynamically.[32] Therefore, the reproducibility of the reaction was quite good compared with that of the conventional hot injection method. The nanostrip product exhibits better spectral qualities and is suitable for industrial application of quantum-confined devices such as color displays or related light-emitting applications (the products obtained by 140 °C reaction exhibited a 462 nm emission wavelength with an FWHM of 13 nm and a 94% PLQY, which meets the required color criteria for primary blue).[32]

2.8. Synthesis of $FAPbBr_3$ by the Modified Hot Injection Method (Samples H1−H8). $FAPbBr_3$ NCs have the potential to be green-emitting materials with PL peaks over 530 nm, and thus, they have been extensively studied. In 2016, Protesescu et al. reported that $FAPbBr_3$ synthesized by a three-precursor hot injection method could achieve 530 nm light emission.[34] The advantage of this method is product tunability through ion stoichiometry, unlike the two-precursor method. The authors performed the synthesis without OLA, which realized the reaction at a lower temperature and eventually solved the problem of thermal instability of organometal halide perovskite. In their study, the PL wavelength was tuned by changing the ratio of lead and bromine. The only complexity of their method is the necessity to use oleylammonium bromide (OLAm-Br) precursor instead of an OLA ligand and a bromine source. In this study, we propose a simpler method to control the reaction by varying the ratio of the formamidinium precursor and lead bromide in the conventional two-precursor method under a constant reaction temperature.

The reaction was conducted by changing the amount of FA-oleate precursor at a reaction temperature of 160 °C (Figure 11). When the reaction temperature was higher than 160 °C, the products decomposed during the reaction. Figure 11a,b shows the PL spectrum change with the volume of injected FA-oleate precursor solution. The concentration of FA-oleate solution was 0.3 mmol/mL. As the amount of FA-oleate precursor increased, the PL spectrum gradually redshifted and the FWHM narrowed. The data indicate that the size of NCs was enlarged and the size distribution decreased.

The reaction with the smallest amount of FA-oleate solution (0.6 mL) produced multiple PL peaks, which is similar to the products synthesized by the hot injection method at a lower temperature. The formation energy of FA perovskites is known to be lower than that of Cs perovskites, i.e., the reaction temperature of 160 °C should be high enough, and the origin of the multiple PL peaks was not the temperature. The TEM images in Figure 11c for NCs synthesized by 0.6 mL of FA-oleate precursor revealed the reason; various sizes of nanocubes and nanoplates were formed, unlike the reaction with 0.8 mL of FA-oleate precursor (Figure 11d). The thickness of the darker nanocubes was larger than that of the other nanoplates.

The mechanism of structural change for $FAPbBr_3$ by varying the amount of FA-oleate precursor was discussed by comparison with Cs perovskites. Both FA and Cs are monovalent cations, and they play the same role in the perovskite structure. However, if the same amount of FA precursor as that of the Cs precursor was added, stable products could not be obtained. For the synthesis of $CsPbBr_3$, the molar ratio of the precursor and the lead bromide precursor should be 0.266; i.e., the reaction proceeds in an environment rich in lead bromide. If the ratio of Cs and Pb is 1, a Cs_4PbBr_6 NC (wide-band gap insulator) is formed instead of $CsPbBr_3$ (although the ratio of Cs and Pb is 4 in theory). This result suggests that Cs_4PbBr_6 is a more stable structure than $CsPbBr_3$.

On the other hand, to form stable $FAPbBr_3$ products, the molar ratio of formamidinium and lead bromide can be close to 1. Even when this ratio was further increased, the obtained product was still fluorescent. This result suggests that $FAPbBr_3$ (luminescent) is more stable than FA_4PbBr_6 (wide-band gap insulator). In fact, we found only one report concerning the synthesis of FA_4PbBr_6, which involved a solid-state reaction and was totally different from the solution-based hot injection method.[41] Our results imply that an excess amount of formamidinium is a driving force for promoting the growth of nanocrystals for the reaction mechanism of $FAPbBr_3$ NCs.

In general, the structural stability of perovskite crystals can be judged simply by the tolerance factor proposed by Goldschmidt in 1926[42]

$$t = \frac{r_A + r_X}{\sqrt{2}(r_B + r_X)} \quad (2)$$

where r_A, r_B, and r_X represent the radius of the A, B, and X ions, respectively, for the perovskite structure ABX_3. The primary function of the A ion is to support and maintain the three-dimensional network structure of the octahedron, and the A ion must match the four adjacent octahedral voids. Twelve adjacent X ions surround each A ion and form a 12-coordinated structure. If the A ion is too large, it cannot be

https://doi.org/10.1021/acsomega.1c05001
ACS Omega 2022, 7, 565−577

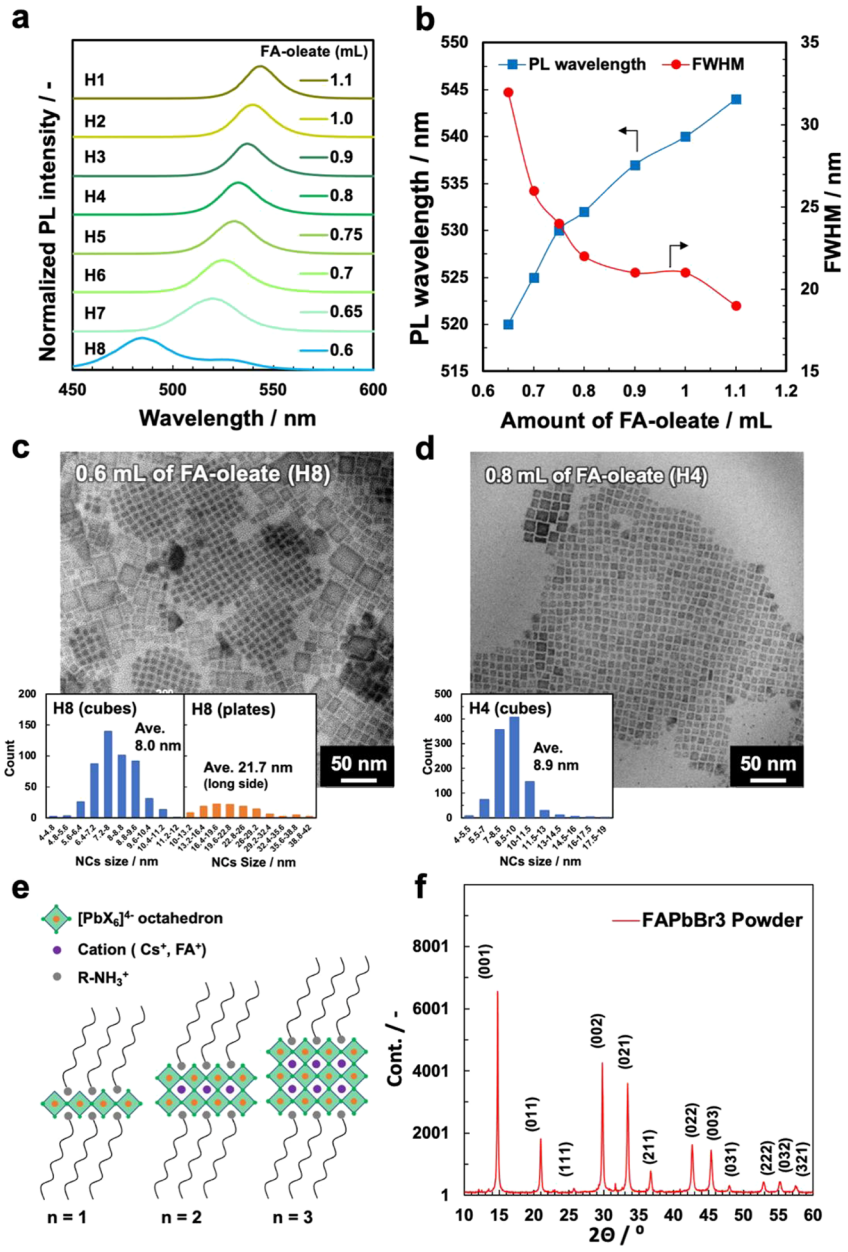

Figure 11. (a) PL spectra and (b) plots of PL wavelength and FWHM against the amounts of FA-oleate precursor for $FAPbBr_3$ NCs. The concentration of FA-oleate solution was 0.3 mmol/mL, and the reaction temperature was 160 °C. With increasing FA precursor amount, the PL wavelength was redshifted and the FWHM was narrowed. (c, d) TEM image of $FAPbBr_3$ NCs synthesized by injection of (c) 0.6 mL (**H8**) and (d) 0.8 mL (**H4**) of FA-oleate solution. The insets are the in-plane size distribution of $FAPbBr_3$ NCs obtained from the TEM image. The size distribution of nanocubes and nanoplates (the long side of the rectangular plates) are shown separately for **H8**. (e) Octahedral layer number (n)-dependent perovskite structures. (f) XRD data of $FAPbBr_3$ NC powder. Absorption spectrum of **H4** is available in Figure S3 in the Supporting Information (**H4**, primary green).

placed in the gap of the octahedral network. If the A ion is too small, it would cause the collapse of the perovskite structure. This semiempirical formula has achieved great success in predicting the stability of perovskite structures and has been widely used to date.

The recent literature points out that octahedrons tend to form a cubic phase structure when $0.9 \leq t \leq 1$. These octahedrons tend to twist and form an orthorhombic phase or a trigonal crystal system when $0.71 \leq t \leq 0.9$.[40] When the tolerance factor cannot satisfy the conditions, the octahedral frame will collapse. Such perovskites have a large band gap, which is basically outside the range of semiconductors.[43] Some lead halide perovskites exhibit a relatively large torsion of the octahedrons, but this does not mean that all these materials have orthorhombic phases.[44−46] For example, bulk $CsPbI_3$ can form a cubic phase crystal structure only when the temperature is higher than 320 °C and can form an orthorhombic phase at room temperature. However, $CsPbI_3$ NCs have a cubic phase crystal structure even at room temperature because of their large surface energy.[35]

The FA^+ cation has a much larger ionic radius than cesium, and the nuclei or small grains tend to decompose during synthesis due to their structural instability. On the other hand, even if the amount of FA ions is close to the critical condition

https://doi.org/10.1021/acsomega.1c05001
ACS Omega 2022, 7, 565−577

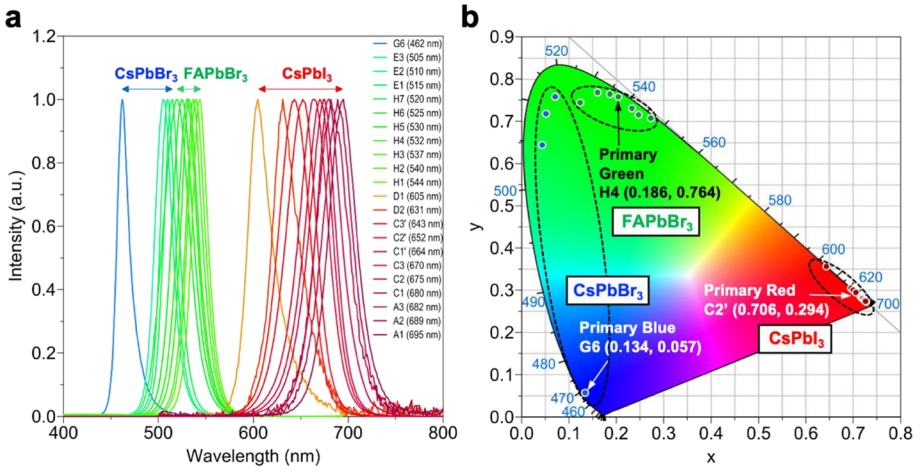

Figure 12. Summary of PL spectra (a) and corresponding color coordinates on a CIE1931 color diagram (b) for the pure-halide perovskite NCs synthesized in this study.

to form stable $FAPbBr_3$ NCs, they could form a low-dimensional structure and stabilize. Figure 11e shows the octahedral layer number (n)-dependent perovskite structures. The ratio of n and the FA layer number should be close to 1 for three-dimensional NCs, but it can be 2 for two-dimensional perovskite NCs (the structure of $n = 1$ does not include FA, so that this is not yet perovskite structure). Conversely, $FAPbBr_3$ NCs with a limited amount of FA ions tend to form a low-dimensional structure. $FAPbBr_3$ NCs are also known to be susceptible to the amount of formamidinium precursor. A change in the mixing ratio of the precursors at ±10% is enough to make a significant difference in terms of their PL spectra. This characteristic of FA perovskites realizes ion stoichiometric tunability of the PL spectra, which did not appear for Cs perovskites (even if the mixing ratio of the precursors was varied within ±20%, the PL spectra of Cs perovskites did not change perceptibly). Figure 11f shows the XRD data of the $FAPbBr_3$ NC powder sample synthesized with 0.8 mL of FA-oleate solution (**H4**), which agrees well with the data of NC cast films[47] and bulk crystals.[48]

3. CONCLUSIONS

In this study, we presented various synthesis pathways of pure-halide perovskite NCs. Although the hot-injection method is still the mainstream approach for synthesizing perovskite NCs due to historical background, it is not necessary to rely on this conventional methodology, and we can challenge the development of a wider range of new synthetic methods to obtain higher-quality perovskite NCs. Eventually, we succeeded in synthesizing perovskite NCs with stable emission of RGB primary colors (Figure 12). The ideal primary color of red at approximately 650 nm was obtained by synthesizing monodispersed $CsPbI_3$ NCs with the conventional hot injection method, but the quality was further improved by the combination of modified hot injection method and centrifugation of a frozen eutectic mixture method (**C2′**). During the process, a new methodology to control the reaction by injecting cationic precursors at low temperatures was also developed and used for the growth of $CsPbBr_3$ nanostrips under thermodynamic control. The development of this slow reaction process at low temperatures suggests the possibility of large-scale batch synthesis in an industrial environment with high reproducibility and spectral quality. The products obtained by the 140 °C reaction exhibited a 462 nm emission, which meets the required color criteria for primary blue (**G6**). For the study of $FAPbBr_3$ NCs, the spectral characteristics of the product were controlled by the amount of FA-oleate precursor. This result evidently showed the ion stoichiometric tunability for FA perovskites, which cannot be achieved for Cs perovskites. Through this approach, an emission wavelength of 532 nm as the primary green emission wavelength was efficiently obtained (**H4**).

Throughout these studies, we have learned the way to design a reliable synthetic route for perovskite NCs according to the desired emission wavelength. Perovskite NCs have excellent performance in their optoelectrical properties.[49] However, their real-world device applications are currently limited by their stability, and this issue must be resolved completely for the universal use of perovskite NC materials.

4. EXPERIMENTAL SECTION

4.1. Material Preparation. Detailed experimental protocol for synthesis of Cs-oleate and FA-oleate precursors as well as $CsPbI_3$ NCs, $CsPbBr_3$ NCs, and $FAPbBr_3$ NCs (hot injection, modified hot injection, and low-temperature mixing and heat-up methods) are available in the Supporting Information.

4.2. Characterization and Instruments. The PL spectra and PLQY of perovskite NCs were obtained under an epifluorescence microscope (ECLIPSE 80i, Nikon, Japan) with a 405 nm diode laser (100 mW (CW), Spectra-Physics, USA) and PMA-12 photonic multichannel analyzer (Hamamatsu, Japan). XRD spectra were obtained using a Bruker D8 Advance diffractometer with Cu K_α radiation (0.15418 nm). Small-angle measurements were taken with a knife edge to minimize background noise. Drop-cast samples were prepared on a silicon substrate. TEM and high-angle annular darkfield (HAADF)−STEM images were obtained with a JEOL JEM-ARM200F microscope with an acceleration voltage of 200 kV. Samples were prepared by drop-casting on a copper grid.

■ ASSOCIATED CONTENT

Supporting Information

The Supporting Information is available free of charge at https://pubs.acs.org/doi/10.1021/acsomega.1c05001.

(Scheme 1) A series of lead-halide perovskite NCs synthesized in this study; detailed synthesis method-

https://doi.org/10.1021/acsomega.1c05001
ACS Omega 2022, 7, 565−577

ology for CS-oleate and FA-oleate precursors, $CsPbI_3$, $CbPbBr_3$ and $FAPbBr_3$ NCs via hot injection, modified hot injection, and low-temperature mixing and heat-up methods; (Figure S1) influence of the reaction temperature for synthesis of $CsPbI_3$ NCs; (Figure S2) influence of the amount of ODE for synthesis of $CsPbI_3$ NCs; (Figure S3) PL and absorption spectra of $CsPbBr_3$ and $FAPbBr_3$ (PDF)

AUTHOR INFORMATION

Corresponding Author

Kaoru Tamada − *Institute for Materials Chemistry and Engineering (IMCE), Kyushu University, Fukuoka 819-0395, Japan; Advanced Institute for Materials Research (AIMR), Tohoku University, Sendai 980-8577, Japan;* orcid.org/0000-0003-2618-9924; Email: tamada@ms.ifoc.kyushu-u.ac.jp

Authors

Junfu Leng − *Institute for Materials Chemistry and Engineering (IMCE), Kyushu University, Fukuoka 819-0395, Japan;* orcid.org/0000-0002-2635-3563

Tian Wang − *Department of Chemistry, National University of Singapore (NUS), Singapore 117543, Singapore*

Zhi-Kuang Tan − *Department of Chemistry, National University of Singapore (NUS), Singapore 117543, Singapore;* orcid.org/0000-0003-1399-1790

Ya-Ju Lee − *Institute of Electro-Optical Engineering, National Taiwan Normal University, Taipei 116, Taiwan;* orcid.org/0000-0002-2663-682X

Chun-Chieh Chang − *Institute of Electro-Optical Engineering, National Taiwan Normal University, Taipei 116, Taiwan;* orcid.org/0000-0003-3728-2454

Complete contact information is available at: https://pubs.acs.org/10.1021/acsomega.1c05001

Notes

The authors declare no competing financial interest.

ACKNOWLEDGMENTS

This work was supported by JSPS KAKENHI grant no. 19H05627 in Japan. J.L. is grateful to the Advanced Graduate Course on Molecular Systems for Devices from the Kyushu University Program for Leading Graduate Schools. J.L. also thanks Dr. Yuko Matsukawa, Kyushu University, for help with the XRD measurements.

REFERENCES

(1) Shirasaki, Y.; Supran, G. J.; Bawendi, M. G.; Bulović, V. Emergence of colloidal quantum-dot light-emitting technologies. *Nat. Photon.* **2013**, *7*, 13−23.

(2) Kim, T. H.; Cho, K. S.; Lee, E. K.; Lee, S. J.; Chae, J.; Kim, J. W.; Kim, D. H.; Kwon, J. Y.; Amaratunga, G.; Lee, S. Y.; Choi, B. L.; Kuk, Y.; Kim, J. M.; Kim, K. Full-colour quantum dot displays fabricated by transfer printing. *Nat. Photon.* **2011**, *5*, 176−182.

(3) Kamat, P. V.; Jara, D. H.; Yoon, S. J.; Stamplecoskie, K. G. Size-dependent photovoltaic performance of $CuInS_2$ quantum dot-sensitized solar cells. *Chem. Mater.* **2014**, *26*, 7221−7228.

(4) Geiregat, P.; Van Thourhout, D.; Hens, Z. A bright future for colloidal quantum dot lasers. *NPG Asia Mater.* **2019**, *11*, 41.

(5) Pietryga, J. M.; Park, Y.-S.; Lim, J. H.; Fidler, A. F.; Bae, W. K.; Brovelli, S.; Klimov, V. I. Spectroscopic and Device Aspects of Nanocrystal Quantum Dots. *Chem. Rev.* **2016**, *116*, 10513−10622.

(6) Smith, A. M.; Nie, S. Semiconductor nanocrystals: structure, properties, and band gap engineering. *Acc. Chem. Res.* **2010**, *43*, 190−200.

(7) Jellicoe, T. C.; Richter, J. M.; Glass, H. F. J.; Tabachnyk, M.; Brady, R.; Dutton, S. E.; Rao, A.; Friend, R. H.; Credgington, D.; Greenham, N. C.; Böhm, M. L. Synthesis and Optical Properties of Lead-Free Cesium Tin Halide Perovskite Nanocrystals. *J. Am. Chem. Soc.* **2016**, *138*, 2941−2944.

(8) Creutz, S. E.; Crites, E. N.; De Siena, M. C.; Gamelin, D. R. Colloidal Nanocrystals of Lead-Free Double-Perovskite (Elpasolite) Semiconductors: Synthesis and Anion Exchange to Access New Materials. *Nano Lett.* **2018**, *18*, 1118−1123.

(9) Wang, Z.; Zhang, X.; Xin, W.; Yao, D.; Liu, Y.; Zhang, L.; Liu, W.; Zhang, W.; Zheng, W.; Yang, B.; Zhang, L. Facile Synthesis of Cu-In-S/ZnS Core/Shell Quantum Dots in 1-Dodecanethiol for Efficient Light-Emitting Diodes with an External Quantum Efficiency of 7.8%. *Chem. Mater.* **2018**, *30*, 8939−8947.

(10) Joon-Suh, P.; Jihoon, K.; Hong Hee, K.; Shinyoung, J.; JoonHyun, K.; Song-ee, L.; Kyu-Tae, L.; Kisun, P.; Barange, N.; JiYeong, H.; Jin Dong, S.; Won Kook, C.; Il Ki, H. Alternative Patterning Process for Realization of Large-Area, Full-Color, Active Quantum Dot Display. *Nano Lett.* **2016**, *16*, 6946−6953.

(11) Schneider, J.; Dudka, T.; Xiong, Y.; Wang, Z.; Rogach, A. L.; Gaponik, N. Aqueous-Based Cadmium Telluride Quantum Dot/Polyurethane/Polyhedral Oligomeric Silsesquioxane Composites for Color Enhancement in Display Backlights. *J. Phys. Chem. C* **2018**, *122*, 13391−13398.

(12) Murray, C. B.; Norris, D. J.; Bawendi, M. G. Synthesis and Characterization of Nearly Monodisperse CdE (E = S, Se, Te) Semiconductor Nanocrystallites. *J. Am. Chem. Soc.* **1993**, *115*, 8706−8715.

(13) Janke, E. M.; Williams, N. E.; She, C.; Zherebetskyy, D.; Hudson, M. H.; Wang, L.; Gosztola, D. J.; Schaller, R. D.; Lee, B.; Sun, C.; Engel, G. S.; Talapin, D. V. Origin of Broad Emission Spectra in InP Quantum Dots: Contributions from Structural and Electronic Disorder. *J. Am. Chem. Soc.* **2018**, *140*, 15791−15803.

(14) Dabbousi, B. O.; Rodriguez-Viejo, J.; Mikulec, F. V.; Heine, J. R.; Mattoussi, H.; Ober, R.; Jensen, K. F.; Bawendi, M. G. (CdSe)ZnS Core−Shell Quantum Dots: Synthesis and Characterization of a Size Series of Highly Luminescent Nanocrystallites. *J. Phys. Chem. B* **1997**, *101*, 9463.

(15) Talapin, D. V.; Mekis, I.; Kornowski, A.; Weller, H.; Götzinger, S.; Benson, O. CdSe/CdS/ZnS and CdSe/ZnSe/ZnS core-shell-shell nanocrystals. *J. Phys. Chem. B* **2004**, *108*, 18826−18831.

(16) Zhu, H.; Prakash, A.; Benoit, D. N.; Jones, C. J.; Colvin, V. L. Low temperature synthesis of ZnS and CdZnS shells on CdSe quantum dots. *Nanotechnology* **2010**, *21*, 255604.

(17) Schmidt, L. C.; Pertegas, A.; Gonzalez-Carrero, S.; Malinkiewicz, O.; Agouram, S.; Espallargas, G. M.; Bolink, H. J.; Galian, R. E.; Perez-Prieto, J. Nontemplate Synthesis of $CH_3NH_3PbBr_3$ Perovskite Nanoparticles. *J. Am. Chem. Soc.* **2014**, *136*, 850−853.

(18) Protesescu, L.; Yakunin, S.; Bodnarchuk, M. I.; Krieg, F.; Caputo, R.; Kovalenko, M. V.; Hendon, C. H.; Yang, R. X.; Walsh, A. Nanocrystals of Cesium Lead Halide Perovskites ($CsPbX_3$, X = Cl, Br, and I): Novel Optoelectronic Materials Showing Bright Emission with Wide Color Gamut. *Nano Lett.* **2015**, *15*, 3692−3696.

(19) Tan, Z.-K.; Moghaddam, R. S.; Lai, M. L.; Docampo, P.; Higler, R.; Deschler, F.; Price, M.; Sadhanala, A.; Pazos, L. M.; Credgington, D.; Hanusch, F.; Bein, T.; Snaith, H. J.; Friend, R. H. Bright light-emitting diodes based on organometal halide perovskite. *Nat. Nanotech.* **2014**, *9*, 687−692.

(20) Zhao, X.; Tan, Z.-K. Large-area near-infrared perovskite light-emitting diodes. *Nat. Photon.* **2019**, *14*, 215−218.

(21) Lin, K.; Xing, J.; Quan, L. N.; de Arquer, F. P. G.; Gong, X.; Lu, J.; Xie, L.; Zhao, W.; Zhang, D.; Yan, C.; Li, W.; Liu, X.; Lu, Y.; Kirman, J.; Sargent, E. H.; Xiong, Q.; Wei, Z. Perovskite light-emitting diodes with external quantum efficiency exceeding 20 percent. *Nature* **2018**, *562*, 245−248.

(22) Cao, Y.; Wang, N.; Tian, H.; Guo, J.; Wei, Y.; Chen, H.; Miao, Y.; Zou, W.; Pan, K.; He, Y.; Cao, H.; Ke, Y.; Xu, M.; Wang, Y.; Yang, M.; Du, K.; Fu, Z.; Kong, D.; Dai, D.; Jin, Y.; Li, G.; Li, H.; Peng, Q.; Wang, J.; Huang, W. Perovskite light-emitting diodes based on spontaneously formed submicrometre-scale structures. *Nature* **2018**, *562*, 249−253.
(23) Nikl, M.; Nitsch, K.; Polak, K.; Polak, K.; Mihokova, E.; Zazubovich, S.; Pazzi, G. P.; Fabeni, P.; Salvini, L.; Aceves, R.; Barbosa-Flores, M.; Perez Salas, R.; Gurioli, M.; Scacco, A. Quantum size effect in the excitonic luminescence of $CsPbX_3$-like quantum dots in CsX (X= Cl, Br) single crystal. *J. Lumin.* **1997**, *7*, 377−379.
(24) Kojima, A.; Teshima, K.; Shirai, Y.; Miyasaka, T. Organometal Halide Perovskites as Visible-Light Sensitizers for Photovoltaic Cells. *J. Am. Chem. Soc.* **2009**, *131*, 6050−6051.
(25) Im, J.-H.; Lee, C.-R.; Lee, J.-W.; Park, S.-W.; Park, N.-G. 6.5% efficient perovskite quantum-dot-sensitized solar cell. *Nanoscale* **2011**, *3*, 4088−4093.
(26) Nedelcu, G.; Protesescu, L.; Yakunin, S.; Bodnarchuk, M. I.; Grotevent, M. J.; Kovalenko, M. V. Fast Anion-Exchange in Highly Luminescent Nanocrystals of Cesium Lead Halide Perovskites ($CsPbX_3$, X = Cl, Br, I). *Nano Lett.* **2015**, *15*, 5635−5640.
(27) Draguta, S.; Sharia, O.; Yoon, S. J.; Brennan, M. C.; Morozov, Y. V.; Manser, J. S.; Kamat, P. V.; Schneider, W. F.; Kuno, M. Rationalizing the light-induced phase separation of mixed halide organic−inorganic perovskites. *Nat. Commun.* **2017**, *8*, 200.
(28) Chen, Z.; Brocks, G.; Tao, S.; Bobbert, P. A. Unified theory for light-induced halide segregation in mixed halide perovskites. *Nat. Commun.* **2021**, *12*, 2687.
(29) Pradhan, B.; Mushtaq, A.; Roy, D.; Sain, S.; Das, B.; Ghorai, U. K.; Pal, S. K.; Acharya, S. Postsynthesis Spontaneous Coalescence of Mixed-Halide Perovskite Nanocubes into Phase-Stable Single-Crystalline Uniform Luminescent Nanowires. *J. Phys. Chem. Lett.* **2019**, *10*, 1805−1812.
(30) Li, G.; Rivarola, F. W. R.; Davis, N. J. L. K.; Bai, S.; Jellicoe, T. C.; de la Peña, F.; Hou, S.; Ducati, C.; Gao, F.; Friend, R. H.; Greenham, N. C.; Tan, Z.-K. Highly Efficient Perovskite Nanocrystal Light-Emitting Diodes Enabled by a Universal Crosslinking Method. *Adv. Mater.* **2016**, *28*, 3528−3534.
(31) Hoke, E. T.; Slotcavage, D. J.; Dohner, E. R.; Bowring, A. R.; Karunadasa, H. I.; McGehee, M. D. Reversible photo-induced trap formation in mixed-halide hybrid perovskites for photovoltaics. *Chem. Sci.* **2015**, *6*, 613−617.
(32) Leng, J.; Wang, T.; Zhao, X.; Ong, E. W. Y.; Zhu, B.; Ng, J. D. A.; Wong, Y.-C.; Khoo, K. H.; Tamada, K.; Tan, Z.-K. Thermodynamic Control in the Synthesis of Quantum-Confined Blue-Emitting $CsPbBr_3$ Perovskite Nanostrips. *J. Phys. Chem. Lett.* **2020**, *11*, 2036−2043.
(33) Akkerman, Q. A.; Park, S.; Brescia, R.; Rastogi, P.; Prato, M.; Manna, L.; Radicchi, E.; Nunzi, F.; Mosconi, E.; De Angelis, F. Nearly Monodisperse Insulator Cs_4PbX_6 (X = Cl, Br, I) Nanocrystals, Their Mixed Halide Compositions, and Their Transformation into $CsPbX_3$ Nanocrystals. *Nano Lett.* **2017**, *17*, 1924−1930.
(34) Protesescu, L.; Yakunin, S.; Bodnarchuk, M. I.; Bertolotti, F.; Masciocchi, N.; Guagliardi, A.; Kovalenko, M. V. Monodisperse Formamidinium Lead Bromide Nanocrystals with Bright and Stable Green Photoluminescence. *J. Am. Chem. Soc.* **2016**, *138*, 14202−14205.
(35) Swarnkar, A.; Marshall, A. R.; Sanehira, E. M.; Chernomordik, B. D.; Moore, D. T.; Christians, J. A.; Luther, J. M.; Chakrabarti, T. Quantum dot-induced phase stabilization of α-$CsPbI_3$ perovskite for high-efficiency photovoltaics. *Science* **2017**, *354*, 92−95.
(36) Liu, F.; Zhang, Y.; Ding, C.; Kobayashi, S.; Izuishi, T.; Nakazawa, N.; Toyoda, T.; Shen, Q.; Ohta, T.; Hayase, S.; Minemoto, T.; Yoshino, K.; Dai, S. Highly Luminescent Phase-Stable $CsPbI_3$ Perovskite Quantum Dots Achieving Near 100% Absolute Photoluminescence Quantum Yield. *ACS Nano* **2017**, *11*, 10373−10383.
(37) Krieg, F.; Rainò, G.; Süess, A.; Grotevent, M. J.; Krumeich, F.; Bodnarchuk, M. I.; Kovalenko, M. V.; Shorubalko, I.; Ong, Q. K.; Stellacci, F.; Burian, M.; Naumenko, D.; Amenitsch, H. Stable ultraconcentrated and ultradilute colloids of $CsPbX_3$ (X = Cl, Br) nanocrystals using natural lecithin as a capping ligand. *J. Am. Chem. Soc.* **2020**, *141*, 19839−19849.
(38) Wang, C.; Jasieniak, J. J.; Chesman, A. S. R. Stabilizing the cubic perovskite phase of $CsPbI_3$ nanocrystals by using an alkyl phosphinic acid. *Chem. Commun.* **2017**, *53*, 232−235.
(39) Imran, M.; Di Stasio, F.; Dang, Z.; Canale, C.; Khan, A. H.; Shamsi, J.; Brescia, R.; Prato, M.; Manna, L. Colloidal Synthesis of Strongly Fluorescent $CsPbBr_3$ Nanowires with Width Tunable down to the Quantum Confinement Regime. *Chem. Mater.* **2016**, *28*, 6450−6454.
(40) Shamsi, J.; Urban, A. S.; Imran, M.; De Trizio, L.; Manna, L. Metal Halide Perovskite Nanocrystals: Synthesis, Post-Synthesis Modifications, and Their Optical Properties. *Chem. Rev.* **2019**, *119*, 3296−3348.
(41) Nguyen, L. A. T.; Minh, D. N.; Yuan, Y.; Samanta, S.; Wang, L.; Zhang, D.; Hirao, N.; Kim, J.; Kang, Y. Pressure-induced fluorescence enhancement of FA α PbBr 2+α composite perovskites. *Nanoscale* **2019**, *11*, 5868−5873.
(42) Goldschmidt, V. Geochemische Verteilungsgesetze der Elemente. *Akad Oslo I Mat-Nat K1* **1926**, *8*, 112−117.
(43) Ju, M. G.; Dai, J.; Ma, L.; Zeng, X. C. Lead-Free Mixed Tin and Germanium Perovskites for Photovoltaic Application. *J. Am. Chem. Soc.* **2017**, *139*, 8038−8043.
(44) Ghosh, S.; Shi, Q.; Paradhan, B.; Kumar, P.; Wang, Z.; Acharya, S.; Pal, S. K.; Pullerits, T.; Karki, K. J. Phonon Coupling with Excitons and Free Carriers in Formamidinium Lead Bromide Perovskite Nanocrystals. *J. Phys. Chem. Lett.* **2018**, *9*, 4245−4250.
(45) Kieslich, G.; Sun, S.; Cheetham, A. K. An extended Tolerance Factor approach for organic-inorganic perovskites. *Chem. Sci.* **2015**, *6*, 3430−3433.
(46) Travis, W.; Glover, E. N. K.; Bronstein, H.; Palgrave, R. G.; Scanlon, D. O. On the application of the tolerance factor to inorganic and hybrid halide perovskites: A revised system. *Chem. Sci.* **2016**, *7*, 4548−4556.
(47) Perumal, A.; Shendre, S.; Li, M.; Tay, Y. K. E.; Sharma, V. K.; Chen, S.; Wei, Z.; Liu, Q.; Gao, Y.; Buenconsejo, P. J. S.; Tan, S. T.; Gan, C. L.; Xiong, Q.; Sum, T. C.; Demir, H. V. High brightness formamidinium lead bromide perovskite nanocrystal light emitting devices. *Sci. Rep.* **2016**, *6*, 36733.
(48) Zhumekenov, A. A.; Saidaminov, M. I.; Haque, M. A.; Alarousu, E.; Sarmah, S. P.; Murali, B.; Dursun, I.; Miao, X.-H.; Abdelhady, A. L.; Wu, T.; Mohammed, O. F.; Bakr, O. M. Formamidinium Lead Halide Perovskite Crystals with Unprecedented Long Carrier Dynamics and Diffusion Length. *ACS Energy Lett.* **2016**, *1*, 32−37.
(49) Yen, M.-C.; Lee, C.-J.; Liu, K.-H.; Peng, Y.; Leng, J.; Chang, T.-H.; Chang, C.-C.; Tamada, K.; Lee, Y.-J. All-inorganic perovskite quantum dot light-emitting memories. *Nature Commun.* **2021**, *12*, 4460.

https://doi.org/10.1021/acsomega.1c05001
ACS Omega 2022, 7, 565−577